ELSEVIER

1 September 2000

Optics Communications 183 (2000) 215–226

OPTICS COMMUNICATIONS

www.elsevier.com/locate/optcom

Mechanisms for multistability in a semiconductor laser with optical injection

Sebastian Wieczorek [a,*], Bernd Krauskopf [b], Daan Lenstra [a]

[a] *Faculty of Sciences, Vrije Universiteit, De Boelelaan 1081, 1081 HV Amsterdam, The Netherlands*
[b] *Department of Engineering Mathematics, University of Bristol, Bristol BS8 1TR, UK*

Received 21 March 2000; received in revised form 2 June 2000; accepted 12 July 2000

Abstract

We perform a detailed study of multistable behaviour in an optically injected semiconductor laser modeled by single-mode three-dimensional rate equations. It turns out that there is a wealth of regions of bi- and multistability – associated with bifurcations of periodic orbits – in the plane of injection strength and injection detuning. We follow such bifurcations over a wide range of parameters, which reveals different mechanisms for multistability in the system. In this way, we find, among others, the coexistence of two different periodic orbits with a chaotic attractor. Our results open new possibilities for optical switching between several different outputs of the laser. © 2000 Elsevier Science B.V. All rights reserved.

PACS: 42.50.Ne; 42.55.Px; 05.45.+b
Keywords: Laser with optical injection; Bifurcation diagram; Optical multistability; Hysteresis

1. Introduction

Semiconductor lasers subject to external optical injection have received a lot of attention, mainly due to applications such as injection locking [1], frequency stabilization [2] and chirp reduction [3]. From a theoretical point of view, a laser with optical injection is the simplest system with interesting dynamics allowing for bifurcation analysis and providing a starting point towards understanding more complicated systems like mutually coupled lasers or lasers with optical feedback. In semiconductor lasers optical injection produces an enormous variety of complicated dynamical behaviour such as undamped relaxation oscillations, quasiperiodicity, routes to chaos via period doubling and the break-up of tori, and homoclinic and heteroclinic bifurcations; see [4] and references therein. More recently, there has been increased interest in these more complicated dynamics in the light of possible applications ranging from chaotic encryption and chaotic synchronization [5] to optical computing [6]. In particular, bistability, that is, the coexistence of two attractors for the same values of the parameters, has been a focus of attention for some time [4,7–13] because switching between outputs with different intensities and spectral properties may find applications in optical communications or logic gates. Bistability between periodic and constant intensity outputs was found in experiments [7,8,12] as well as in numerical studies [7,9]

* Corresponding author. Tel.: +31-20-444-7860, fax: +31-20-444-7899; e-mail: sebek@nat.vu.nl

PII: S0030-4018(00)00867-1

and in theoretical work [13]. It was also reported that an injected laser may exhibit coexistence of conservative and dissipative behaviour [14].

In this paper we attempt to give a global view on bistability and, in fact, multistability in the laser with injection by revealing and computing curves of bifurcations that lead to additional attractors. In this way, we systematically find regions of multistability between many other kinds of operation, such as quasiperiodic oscillations, periodic signals of very high period and chaos. This is highlighted by the two examples in Figs. 1 and 2. Fig. 1(a) shows three simultaneous attractors, namely a running phase solution [Fig. 1(b)], a periodic solution [Fig. 1(c)] and quasiperiodic motion on a torus [Fig. 1(d)]. Multistability can also be found in the presence of chaotic attractors, as is shown in Fig. 2(a), where the three simultaneous attractors are two different periodic orbits [Fig. 2(b) and (c)] and a chaotic attractor [Fig. 2(d)]. Which of the attractors the system settles down to depends on the initial condition. Furthermore, when a parameter is swept gradually through a region of multistability then one will find hysteresis loops with sudden jumps from one attractor to another at different values of the parameter, depending on the direction of the sweep.

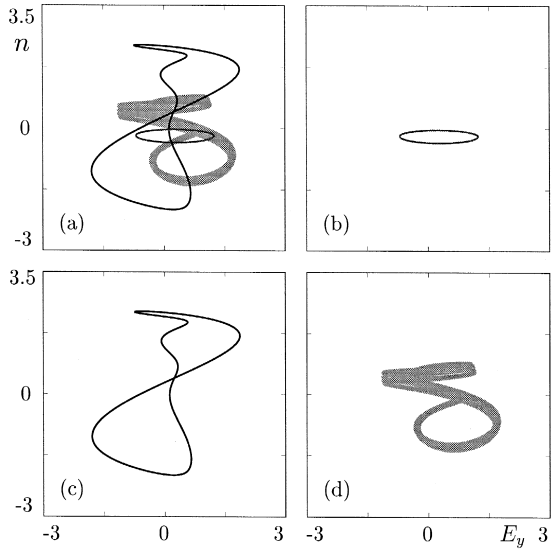

Fig. 1. For $K = 0.743$ and $\omega = -2.93$ there is multistability between three different attractors (a), namely the running phase solution (b), a large periodic orbit (c), and quasiperiodic motion on a torus.

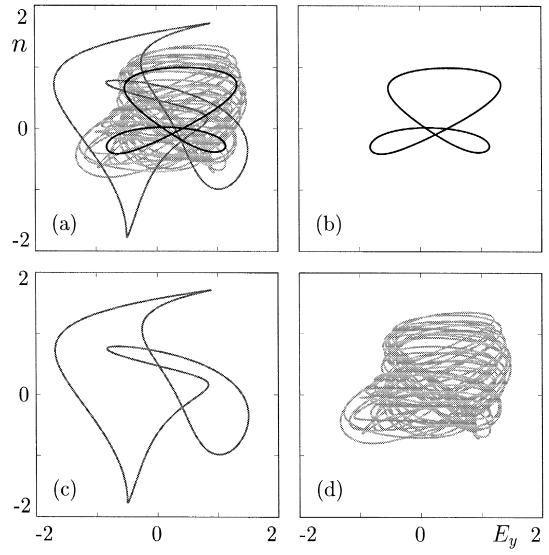

Fig. 2. For $K = 0.29$ and $\omega = -1.36$ there is multistability between three different attractors (a), namely a periodic orbit of period two (b), a periodic orbit of period three (c), and a chaotic attractor (d).

We would like to point out that we identified these cases of multistability not by coincidence, but instead by systematic investigation as a necessary step on the route from the running phase solution to locking of the laser; see Section 3 for details. In fact, multistability should not be seen as an isolated phenomenon, but as an integrated part of the bifurcation diagram of the system. This point of view allows us to identify multistability as part of a consistent picture. With powerful methods from bifurcation theory we explore this picture and identify mechanisms that create particular attractors. This provides new insight into the origin of multistability in the laser with injection. The two mechanisms we found for multistability are a supercritical saddle-node of limit cycle bifurcation and a subcritical torus bifurcation, and this is explained in Section 3.

The paper is organized as follows. In Section 2 we introduce the rate equations, discuss the different bifurcations and explain how they may contribute to multistability. Examples of multistable behaviour are presented in Section 3, where we show how they

occur naturally in the transition to locking. Conclusions are drawn in Section 4.

2. Background on the bifurcation diagram

For a single-mode diode laser with monochromatic optical injection the original *three-dimensional* rate equations for the slowly varying complex electric field $E = E_x + \mathrm{i}E_y$ and the normalized inversion n are given by [4]

$$\dot{E} = K + \left(\tfrac{1}{2}(1+\mathrm{i}\alpha)n - \mathrm{i}\omega\right)E,$$

$$\dot{n} = -2\Gamma n - (1+2Bn)\left(|E|^2 - 1\right). \qquad (1)$$

The optical reference frequency with respect to which Eqs. (1) are formulated is the injected optical frequency [4]. There are five parameters of which the injected field strength K and the detuning of the injected field from the solitary laser frequency ω are most important because they can be changed during an experiment. The parameters B and Γ represent material properties of the laser and are fixed to the realistic values $B = 0.015$ and $\Gamma = 0.035$. The parameter α is the linewidth enhancement factor. We focus on the case $\alpha = 2$ throughout this paper, but would like to stress that multistability can be found in the same way for other values of α.

To facilitate the interpretation of our results from the experimental point of view [10,19] we now explain how to translate the scaled quantities from Eqs. (1). The power of the injected field P_{inj} and its frequency ω_{inj} are

$$P_{\mathrm{inj}} = K^2\left(\frac{\omega_R}{\kappa}\right)^2 \frac{R_1}{(1-R_1)^2}P_0, \quad \omega_{\mathrm{inj}} = \omega\omega_R + \omega_{\mathrm{sol}}. \qquad (2)$$

Here R_1 is the power reflectivity of the laser's facet through which light is injected, ω_R and ω_{sol} are the relaxation oscillation and solitary laser frequencies of the free running laser, while κ is the injected field rate. Furthermore, P_0 is the power that the free running laser emits through the facet R_1. Eqs. (1) are scaled in such a way that the free running laser is assumed to operate above threshold. The pump current is then incorporated into K, meaning that increasing K corresponds to either increasing the amount of injection or decreasing the pump current; see Section 2 in [4] for further details.

We look at Eqs. (1) in the same spirit as in our earlier work [4] which serves as a basis for this study. The special merit of our method is that we compute bifurcations with the package AUTO [15] directly, without the necessity of integrating Eqs. (1). The package AUTO enables us to follow stationary points and periodic orbits as a parameter is varied and then to detect when a bifurcation, that is, a qualitative change of the dynamics, takes place. It is then possible to follow this bifurcation in two parameters, in our case in K and ω; for a more detailed explanation of this method called continuation see [16] and [15] and further references therein. In this way, we detect bifurcations of stationary points and periodic orbits and follow them in the (K,ω)-plane, which results in a picture of regions of different dynamics in phase space; see also [4]. This approach is more accurate and less time consuming than trying to find regions of different dynamics by numerical simulation of Eqs. (1), and most importantly, it is a systematic method taking advantage of inherent properties of the system. Notice that identifying regions of multistability by simulation requires trying a large number of initial conditions, and some attractors may still be overlooked.

System (1) has an amazing complexity of bifurcations. We do not show all of them here, but present in Fig. 3 the most important bifurcations that form the backbone of the dynamics; see [4] for more details. In Section 3 we will focus on additional bifurcation curves producing multistability in the system. The bifurcation curves in Fig. 3 divide the (K,ω)-plane into regions of different dynamics. Each point in this plane corresponds to a particular phase portrait, which may contain more than one attractor. If parameters are changed so that a bifurcation curve is crossed then the phase portrait will change qualitatively. We also distinguish between sub- and supercritical bifurcations. Black parts of bifurcation curves correspond to supercritical bifurcations in which attractors bifurcate and grey parts correspond to subcritical bifurcations of repelling objects. Subcritical bifurcations are less important from an experimental point of view but we trace them out as they may produce stable objects (for instance in a subcritical

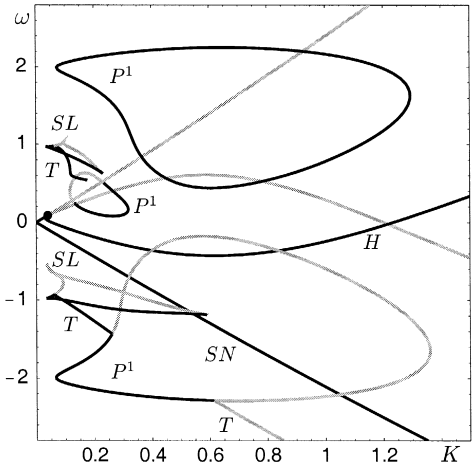

Fig. 3. The bifurcations of stationary points (a) and limit cycles (b) in the (K,ω)-plane that form the backbone of the bifurcation diagram.

torus bifurcation) or change to supercritical. Notice that the bifurcation curves are interlinked and organized into a complicated web. We now discuss the different bifurcations in some detail; as a general reference see for example [16].

There are two bifurcations of stationary points, namely the saddle-node bifurcation *SN* and the Hopf bifurcation *H*. In the saddle-node bifurcation two stationary points are created that exist inside the triangle-shaped region bounded by *SN*. When the black part of *SN* is crossed one of the bifurcating stationary points is an attractor. It physically corresponds to the laser operating at constant power and at the frequency of the injected light, meaning that the laser locks to the input signal. On the other hand, along the gray part of the curve *SN* a repellor and a saddle point bifurcate, an event that is not noticed in experiment or numerical simulation. In fact, there is a global structure involved in the saddle-node bifurcation [4]: the two stationary points are born on a limit cycle. The limit cycle exists for $K = 0$ and its period goes to infinity as *SN* is approached. However, this is not the case for large values of the detuning ω (after a codimension-two homoclinic saddle-node bifurcation point on *SN*). In the Hopf bifurcation a stationary point changes its stability, which gives rise to a periodic orbit. Along the black part of *H* an attracting periodic orbit is born from the attracting stationary point, and this corresponds physically to the undamping of the relaxation oscillation.

The running phase solution that exists for small *K*, as well as the periodic orbit born on the Hopf curve *H*, can undergo a number of bifurcations. A periodic orbit may double its period, give rise to a torus or disappear (or appear) in a saddle-node of the limit cycle bifurcation. We detect and follow these bifurcations in the (K,ω)-plane. Curves of period-doubling bifurcations are denoted by P^1 and usually form the first step in a period-doubling cascade to chaos. From the point of view of multistability, a very important bifurcation is the *saddle-node of limit cycle* bifurcation, which results in the creation (or destruction) of two periodic orbits. Curves of saddle-nodes of limit cycles are marked by *SL*. A saddle and an attracting limit cycle bifurcate in the supercritical case (black curve), and a saddle and repelling limit cycle bifurcate in the subcritical case (grey curve). The supercritical case generates an extra attracting orbit, and it is one of the important mechanism leading to bi- or multistability in the system. Physically, the appearance of a new orbit means that some resonance in the laser gets excited, often because the operational parameters *K* and ω drive the laser close to its relaxation frequency or multiples thereof. For example in Fig. 3 the two saddle-node of limit cycle bifurcation curves starting with a cusp at $\omega \approx \pm 1$ represent a resonance between the relaxation oscillation frequency of the laser and the detuning of the injected light from the free running laser frequency.

Finally, in a torus bifurcation (Neimark–Sacker bifurcation of the Poincaré map) a periodic orbit changes its stability and gives rise to a torus. Along the black part of a torus curve *T* the bifurcating torus is attracting, and along a grey part it is repelling. In the subcritical case (along a gray part of *T*) a repelling limit cycle becomes attracting and gives rise to a repelling torus. That means that an extra attractor appears in the system and this may contribute to bi- or multistability. which constitute a second mechanism for multistability. Note as a reminder that the dynamics on the torus can be locked or quasiperiodic, depending on whether the rotation number is rational or not. From a physical point of view the torus curves *T* which start from curves *SL* at $\omega \approx \pm 1$ in Fig. 3 represent competition between

the relaxation oscillation frequency and the detuning of the injected light from the free running laser frequency with many sub- and superharmonic resonances which are not indicated in Fig. 3.

Note that in Fig. 3 we do not show all bifurcation curves in order to keep the figure simple. In the next section, we will show additional bifurcation curves that are necessary to understand the occurrence of multistability in the transition to locking.

3. Mechanisms for multistability

The bifurcation diagram in Fig. 3 already hints at the presence of regions with several coexisting attractors and we will now study this in much more detail. To this end, we concentrate on the particularly important transition from the running phase solution that exists for small K to stable locking for larger values of K. The exact nature of this transition depends crucially on the value of the detuning ω [17]. To study how multistability appears we fix the detuning ω to representative values and increase the injection strength K. The transition and the occurrence of multistability is then shown by a sequence of phase portraits, which were computed with the package DsTool [18]. At the same time, we show the extra bifurcation curves in the (K,ω)-plane that are needed to understand the bifurcations we encounter in this transition. Effectively we perform a cross section through the bifurcation diagram, and we indicate this clearly in the figures that follow.

For very low injection strength there is only one attractor, namely a limit cycle which is called the running phase solution. It is a continuation of the constant intensity steady state of the free running laser (without injection). Physically, the running phase solution represents the laser operating at the free running laser frequency shifted due to injection. When the injection strength K is increased an enormous variety of bifurcations appear until finally the locking regime is reached where an attracting stationary point exist. The running phase solution may double its period, become a torus or transform into a chaotic attractor which subsequently disappears. In the mean time, new objects may arise which contribute to multistability and participate in the final bifurcation to locking. Here we will demonstrate that multistability is a natural part of this process.

There is a region in the (K,ω)-plane where the running phase solution coexists with a stationary point, and this was recently studied theoretically and in experiments [8,11–13]. We start with this example as it is the simplest case of bistability in the system and allows for a nice comparison between our approach and asymptotic formulas derived in [11,13]. This bistability occurs for negative values of ω below the point $\omega \approx -9.3$ where the gray torus bifurcation curve T crosses the saddle-node bifurcation curve SN; see the bifurcation diagram in Fig. 4. At the moment we discuss what happens below the crossing point. In order to discuss the dynamics above $\omega \approx -9.3$ we need to introduce more bifurcation curves, which is done in the next paragraphs of this section. In the region below the crossing point at $\omega \approx -9.3$ of SN and T the attracting stationary point born on SN coexists with the running phase solution which disappears only on T. To illustrate this we show representative phase portraits projected onto the complex E-plane in Fig. 4 for fixed $\omega = -12$ and increasing injection strength K, which corresponds to moving along the dashed line in the bifurcation diagram. For small K there is only the running phase solution [Fig. 4(a)]. When K is increased the saddle-node bifurcation SN is crossed which generates an attracting stationary point [Fig. 4(b)] leading to bistability. The two attractors coexist up to the moment when the torus bifurcation T is reached and the running phase solution disappears [Fig. 4(c)]. From now on we are left with a stable stationary point as the only attractor – the laser is locked. Notice that this happens for large negative detunings ω where no attracting limit cycle is involved in the saddle-node bifurcation. This bistability leads to a hysteresis loop when K is swept back and forth through the bifurcation values. When increasing K one follows the unlocked running phase – without noticing the creation of a stable point on SN – up to the torus bifurcation, where there is an abrupt jump to the locked solution. However, when decreasing K from the locked solution the emergence of the running phase solution on T will be missed. Instead one will observe a sudden jump to the running phase solution at SN where the locked

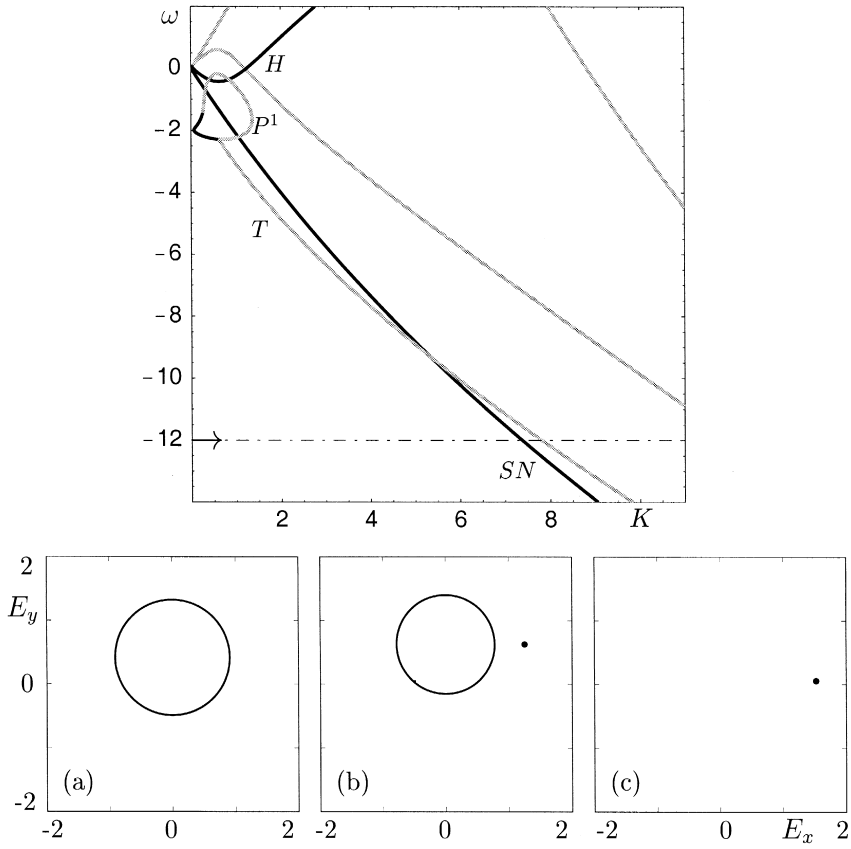

Fig. 4. Bifurcation diagram in the (K,ω)-plane showing how the torus bifurcation curve T crosses the saddle-node bifurcation curve SN. This opens up a region of bistability between a stationary point and a limit cycle. The respective attractors are shown in panels (a) through (c) as projections onto the (E_x,E_y)-plane. $\omega=-12$ and from (a) to (c) K takes the values: 5, 7.5, and 9.

solution disappears. This is a classic example of hysteresis which has been brought out nicely in [8].

We now show that the transition to locking and the ensuing multistability can be much more complicated. Fig. 5 presents the transition to locking for a fixed positive detuning of $\omega=0.85$. This corresponds to the cross section through the bifurcation diagram along the dashed line; for higher values of the injection K we refer to Fig. 3. Corresponding phase portraits along this transition are shown as projections onto the complex E-plane, where the origin is marked with a cross. This makes it easy to distinguish between running phase solutions, which surround the origin, and relaxation oscillations, which do not. For small values of K the running phase solution is the only attractor [Fig. 5(a)]. An attracting torus is born when the curve T is crossed [Fig. 5(b)]. When K is increased further, the dynamics on the torus locks, which means that there is an attracting limit cycle on the torus [Fig. 5(c) and (d)]. In other words, a resonance tongue (not shown in the bifurcation diagram in Fig. 5) was entered. At some point the black part of the saddle-node of limit cycle bifurcation curve SL is crossed and an extra attracting limit cycle appears [Fig. 5(c)] that coexist with the locked orbits on the torus [Fig. 5(c) and (d)]. This is an example of how a saddle-node of limit cycle bifurcation leads to multistability. With a further increase of K the torus breaks up into a chaotic attractor and the periodic orbit coexist with chaos [Fig. 5(e)]. Next, the chaotic attractor disappears [Fig. 5(f)] and then the periodic orbit period-doubles

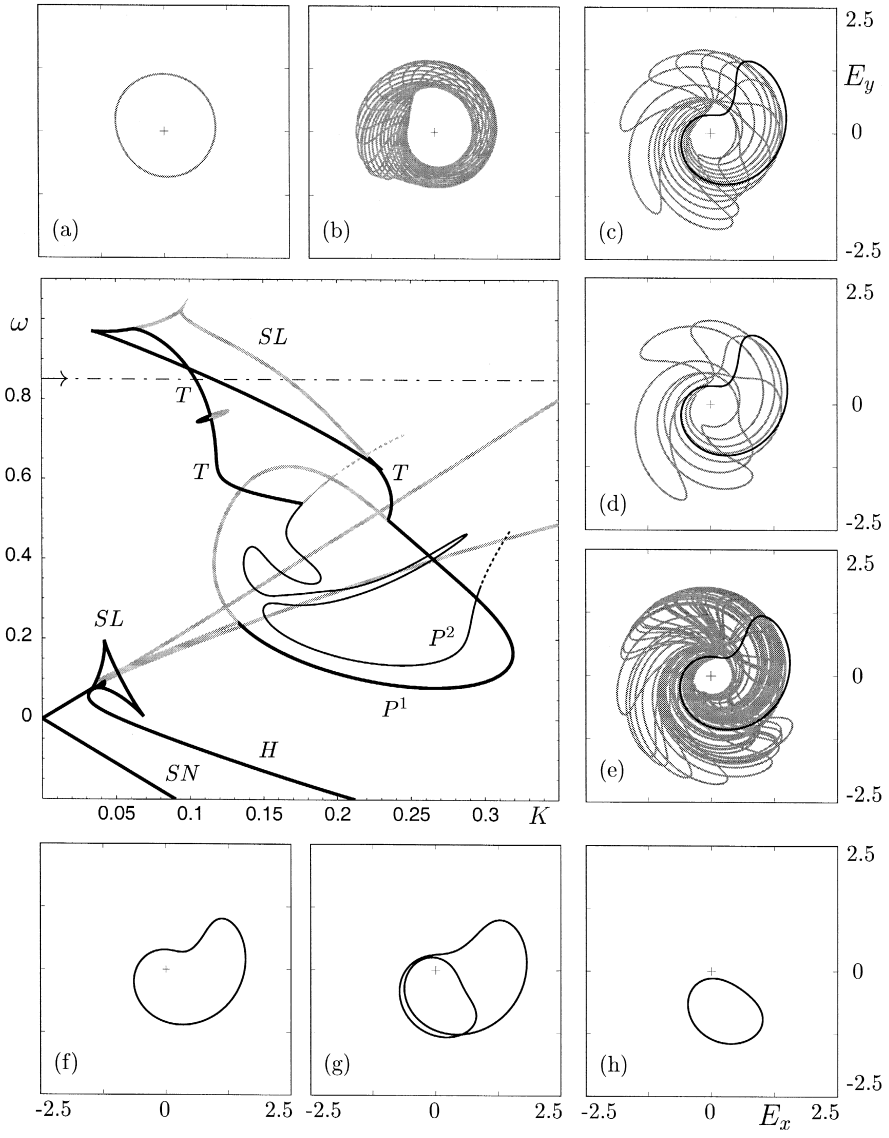

Fig. 5. Bifurcation diagram in the (K,ω)-plane together with representative phase portraits for fixed $\omega = 0.85$ and changing K as indicated by the dashed line. Shown are projections of attractors onto the (E_x,E_y)-plane. Different attractors are distinguished by different shades of gray. From (a) to (h) K takes the values: 0.05, 0.106,0.117, 0.118, 0.123, 0.13, 0.4 and 1.1.

when the big black curve P^1 in Fig. 3 is crossed [Fig. 5(g)]. For a yet higher value of K there is an inverse period-doubling, again on crossing the big black curve P^1 in Fig. 3, after which the limit cycle shrinks in size [Fig. 5(g)]. It finally disappears in the Hopf bifurcation on the black branch of the curve H, after which the only attractor is an attracting stationary point so that the laser is locked to the input.

If we follow the running phase solution by increasing K for fixed $\omega = -1.36$ we observe multistability not only due to a saddle-node of limit cycle bifurcation, but also due to a subcritical torus bifurcation. This transition corresponds to the dashed cross section through the bifurcation diagram shown in Fig. 6. Starting from the running phase solution [Fig. 6(a)], first we cross the gray part of SL^2 (but

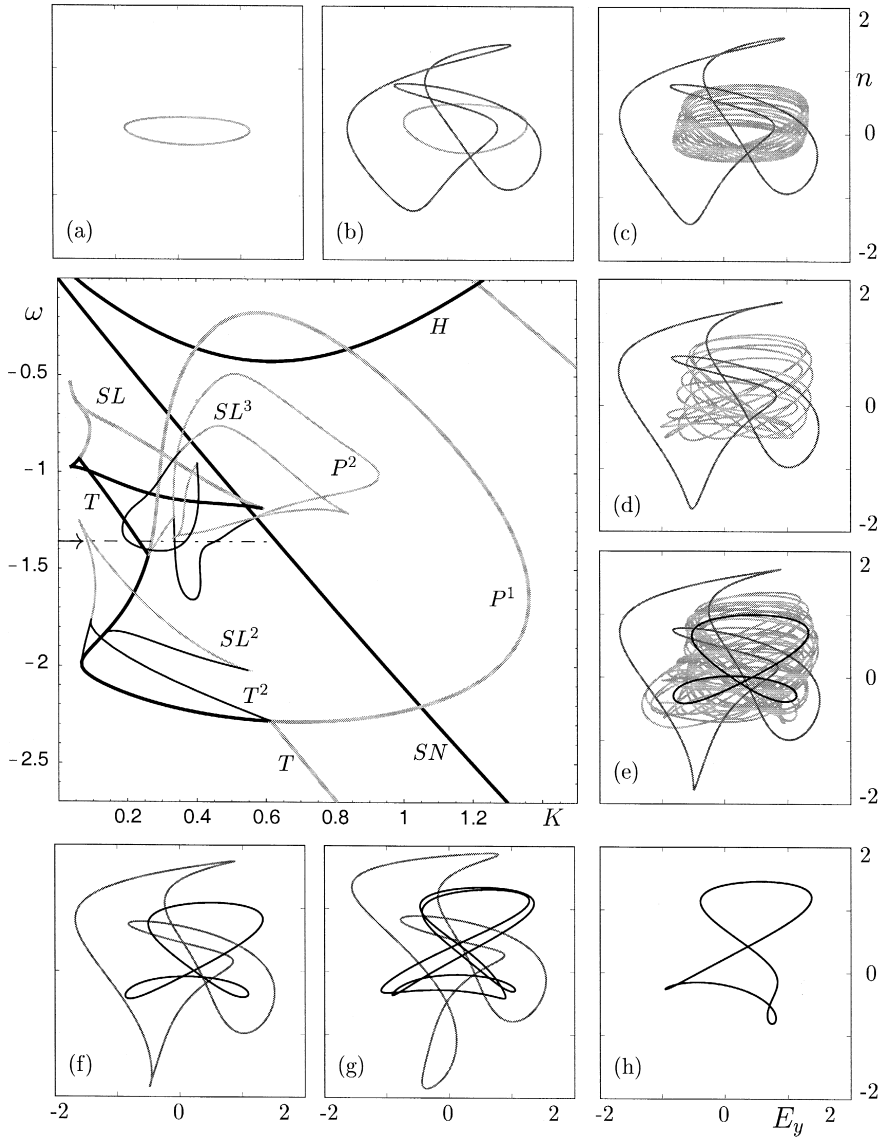

Fig. 6. Bifurcation diagram in the (K,ω)-plane together with representative phase portraits for fixed $\omega = -1.36$ and changing K as indicated by the dashed line. Shown are projections of attractors onto the (E_y,n)-plane. Different attractors are distinguished by different shades of gray. From (a) to (h) K takes the values: 0.1, 0.22, 0.24, 0.27, 0.29, 0.3, 0.44, and 0.48.

this will not be observed). Then the saddle-node of limit cycle isola SL^3 is crossed, where a limit cycle is born that has three times the basic period. This new period-three orbit coexist with the running phase solution [Fig. 6(b)]. Next, the running phase solution becomes repelling and it gives rise to an attracting torus [Fig. 6(c)] when the black curve T is crossed. The dynamics on the torus then locks to a high-period attracting orbit [Fig. 6(d)]. When K is increased further the repelling running phase doubles its period on the gray part of P^1. Notice that this bifurcation does not concern attracting objects and is not visible in the phase portrait panels where we only plot attractors. The next bifurcation is the subcritical torus bifurcation of the limit cycle whose period is twice the basic period. It takes place along the short,

gray torus curve which starts from where the black curve T connects to P^1 (called a 1:2 resonance point). In this bifurcation a period-two, unstable running phase solution becomes attracting by giving rise to an unstable torus. That is how an extra attracting orbit of twice the basic period appears, so that we now have the coexistence of two periodic orbits and a chaotic attractor [Fig. 6(e)] that appeared through the break up of the attracting torus [in panels Fig. 6(c) and (d)]. This is exactly the instance of multistability that was illustrated in Fig. 2. Next the chaotic attractor disappears [Fig. 6(f)] and the attracting orbit goes through the period doubling bubble P^2 [Fig. 6(g)]. Going further, SL^3 is crossed again and the period-three orbit disappears [Fig. 6(h)]. The remaining limit cycle increases its period to infinity as the black branch of SN is approached [Fig. 6(h)] and then it disappears on SN when an attracting stationary point is born on the limit cycle and the laser becomes locked.

A different situation is present for a detuning ω smaller than -2.3, but above the crossing point $\omega \approx -9.3$ of the two bifurcation curves SN and T; compare Figs. 6 and 4. There exist an attracting orbit inside a repelling torus on the left side of the subcritical curve T. As T is approached from the left, the repelling torus shrinks onto the attracting orbit. The orbit becomes repelling after T is crossed and the repelling torus disappears. In the saddle-node bifurcation SN another attracting orbit disappears. This means that there must be *two* attracting orbits on the left side of T. Because the running phase solution is

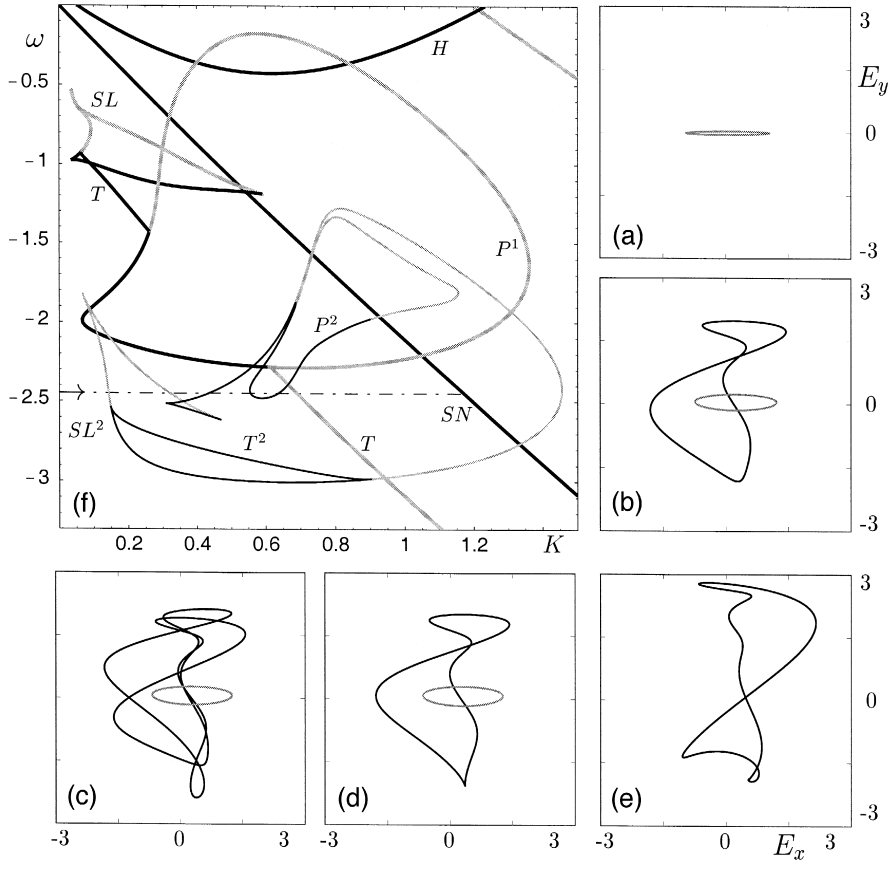

Fig. 7. Bifurcation diagram in the (K,ω)-plane together with representative phase portraits for fixed $\omega = -2.48$ and changing K as indicated by the dashed line. Shown are projections of attractors onto the (E_y,n)-plane. Different attractors are distinguished by different shades of gray. From (a) to (f) K takes the values: 0.1, 0.5, 0.6, 0.65 and 1.17.

the only attractor for very low values of K the other attracting limit cycle must be born somewhere on the way to locking. Following the nature of the problem we found a saddle-node of limit cycle bifurcation which generates the 'missing' limit cycle. The corresponding bifurcation curve SL shown in Fig. 7 turns out to be an isola with the torus bifurcation curve T^2 and the period-doubling bifurcation curve P^2 attached to it. If we increase the injection strength K for fixed $\omega = -2.45$, as is indicated by the dashed line in Fig. 7, then the running phase solution [Fig. 7(a)] is the only attractor up to the moment when we cross the black part of SL^2. An attracting orbit of twice the basic period is born in this bifurcation and we have bistability [Fig. 7(b)]. Increasing K further, the black part of P^2 is crossed and the limit cycle

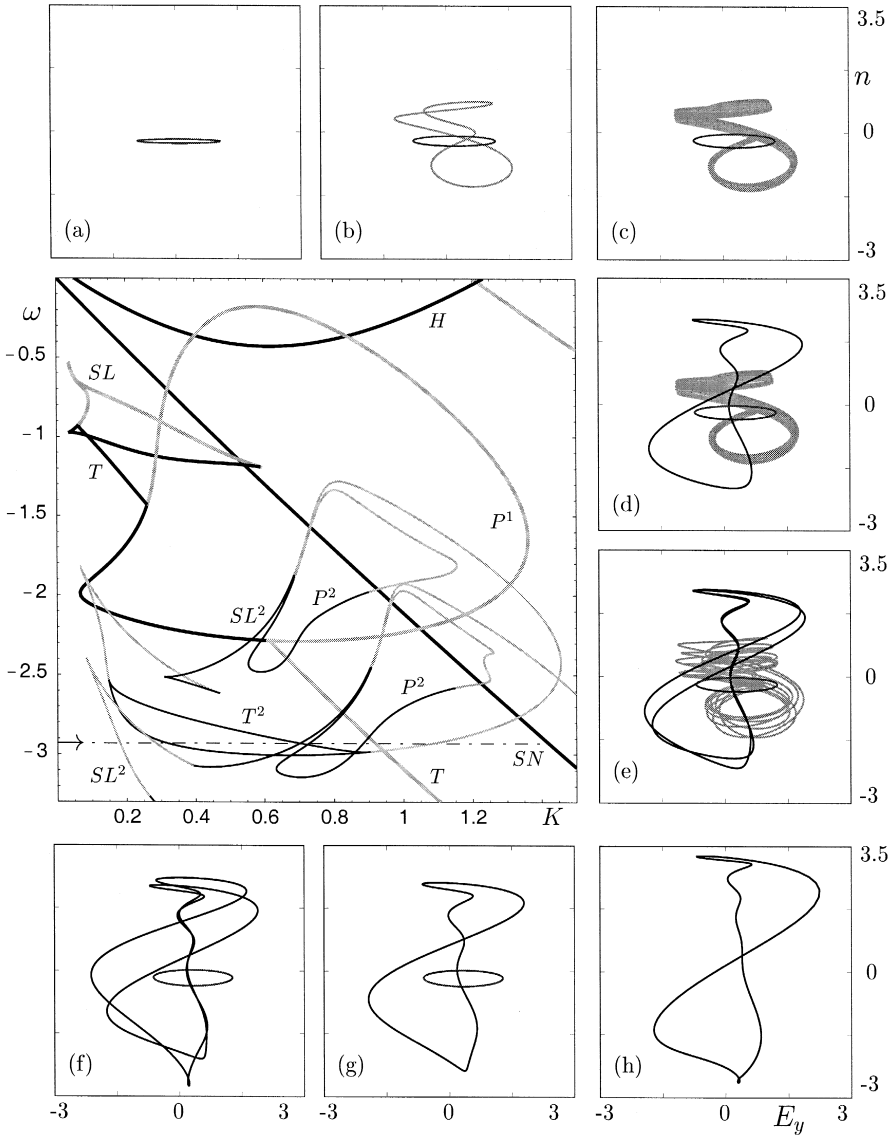

Fig. 8. Bifurcation diagram in the (K,ω)-plane together with representative phase portraits for fixed $\omega = -2.93$ and changing K as indicated by the dashed line. Shown are projections of attractors onto the (E_y,n)-plane. Different attractors are distinguished by different shades of gray. From (a) to (h) K takes the values: 0.2, 0.5, 0.705, 0.71, 0.735, 0.88, 0.89, and 1.4

born on SL^2 doubles its period [Fig. 7(c)] and later undergoes an inverse period-doubling [Fig. 7(d)]. The two orbits coexist until the gray torus bifurcation curve T is reached where the running phase solution disappears. From there on, we have one attracting orbit [Fig. 7(e)] whose period goes to infinity as SN is approached. After crossing SN the laser is locked.

If we look at the bifurcation diagram in Fig. 7 for ω values smaller than -2.9 (but still above $\omega \approx -9.3$) then we notice that there is the same problem as previously. We need to find out where the second attracting orbit is generated that bifurcates on SN. Again, we find another saddle-node of limit cycle bifurcation curve which is presented in Fig. 8. The bifurcation diagram in Fig. 8 is more complicated, because we added more bifurcation curves that are necessary to understand the transition to locking for a fixed detuning of $\omega = -2.93$. This reveals some regions where more then two different attractors coexist. Starting with the running phase solution [Fig. 8(a)] and increasing K leads to crossing the saddle-node of limit cycle curve SL^2 where an attracting orbit of twice the basic period is born [Fig. 8(b)]. Increasing K further we cross the torus bifurcation curve T^2 where the periodic orbit coming from SL^2 bifurcates to a torus [Fig. 8(c)]. Next a second curve SL^2 is crossed and an attracting limit cycle is born which coexist with the torus and the running phase solution [Fig. 8(d)]. This is the example of multistability that we used for illustration in Fig. 1. The dynamics on the torus then locks (a resonance tongue was entered) and the orbit born on the second curve SL^2 undergoes period-doubling on P^2 [Fig. 8(e)]. Then, as K is increased further, the torus breaks up and disappears [Fig. 8(f)]. The orbit that was born on the second curve SL^2 undergoes an inverse period-doubling bifurcation [Fig. 8(g)], and then the running phase solution disappears in the torus bifurcation T [Fig. 8(h)]. The remaining limit cycle disappears at SN after which the laser locks to the input signal.

The above cases clearly show that there are two mechanisms leading to multistability in the system: the supercritical saddle-node of limit cycle bifurcation and the subcritical torus bifurcation. The transition to locking generally involves a complicated interplay between these mechanisms and other bifurcations, which naturally gives rise to multistability. Indeed multistability is not an isolated phenomenon, but an integral part of the intricate pattern of interlinked bifurcations that constitute the bifurcation diagram of the laser with optical injection.

From an experimental point of view the dynamics of semiconductor lasers is examined mostly by looking at RIN spectra or optical spectra [19]. In an experiment multistability shows up as an abrupt change in the observed spectra. There are two possibilities. First, a spectrum can jump erratically between two spectra for fixed parameter values, and this corresponds to the coexistence of attractors and jumps between them due to noise. Second, an abrupt change in the spectrum may occur when parameters are changed. To test for bi- or multistability one would have to sweep parameters back and forth and check for hysteresis effects, that is, for changes in the spectrum occurring at different parameter values. Abrupt jumps in spectra indicating coexisting attractors have been seen in experiments [20].

4. Conclusions

We gave a global view on multistability, that is, the coexistence of different attractors, in the full three-dimensional rate equation model describing a semiconductor laser with optical injection. Methods from bifurcation theory allowed us to identify new regions in parameter space where two and even three different attractors, such as stationary points, limit cycles of several periods, quasiperiodic oscillations and chaos, coexist. It turns out that multistability is a necessary ingredient in different possible transitions from a running phase solution to locking as the injection strength is increased for different (but fixed) values of the detuning. Our findings agree with existing experimental and theoretical results and predict new dynamical behavior which has not been observed yet. We expect that some of the multistabilities we found along the route to locking will manifest itself as clear hysteresis loops in experiments.

We identified coexisting attractors of very different nature in terms of the intensity output and spectral properties of the laser. This may be useful for new applications. Switching between a periodic orbit and the locked solution or between two periodic

orbits of different intensity may find application in optical gates, while switching between a periodic orbit and a chaotic attractor may be interesting for optical communication combined with chaotic encryption.

Acknowledgements

This research was supported by the Foundation for Fundamental Research on Matter (FOM), which is financially supported by the Netherlands Organization for Scientific Research (NWO).

References

[1] R. Lang, IEEE J. Quantum Electron. 18 (1982) 976.
[2] S. Kobayashi, T. Kimura, IEEE J. Quantum Electron. 16 (1980) 915.
[3] F. Mogensen, H. Olesen, G. Jacobsen, Electron. Lett. 21 (1985) 696.
[4] S.M. Wieczorek, B. Krauskopf, D. Lenstra, Opt. Commun. 172 (1999) 279.
[5] C.R. Mirasso, P. Colet, P. Garcia-Fernández, IEEE Photon. Techn. Lett. 8 (1996) 299.
[6] S. Sinha, W.L. Ditto, Phys. Rev. Lett. 81 (1998) 2156.
[7] A. Gavrielides, V. Kovanis, P.M. Varangis, T. Erneux, G. Lythe, Quant. Semiclass. Opt. 9 (1997) 785.
[8] J.M. Liu, H.F. Chen, X.J. Meng, T.B. Simpson, IEEE Photon. Techn. Lett. 9 (1997) 1325.
[9] P.C. de Jagher, W.A. van der Graaf, D. Lenstra, Quant. Semiclass. Opt. 8 (1996) 805.
[10] V. Kovanis, A. Gavrielides, T.B. Simpson, J.M. Liu, Appl. Phys. Lett. 67 (1995) 2780.
[11] V. Kovanis, T. Erneux, A. Gavrielides, Opt. Commun. 159 (1999) 177.
[12] S.K. Hwang, J.M. Liu, Opt. Commun. 169 (1999) 167.
[13] M. Nizette, T. Erneux, A. Gavrielides, V. Kovanis, Injection locked semiconductor laser dynamics from large to small detunings, Proc. SPIE 3625 (1999).
[14] A. Politi, G.L. Oppo, R. Badii, Phys. Rev. A 33 (1986) 4055.
[15] E. Doedel, T. Fairgrieve, B. Sandstede, A. Champneys, Yu. Kuznetsov, X. Wang, AUTO 97: Continuation and bifurcation software for ordinary differential equations, http://indy.cs.concordia.ca/auto/main.html.
[16] Yu.A. Kuznetsov, Elements of Applied Bifurcation Theory, Applied Mathematical Sciences, Vol. 112, Springer, Berlin, 1995.
[17] D. Lenstra, G.H.M. Tartwijk, W.A. van der Graaf, P.C. De Jagher, Chaos in Optics, Proc. SPIE 2039 (1993).
[18] A. Back, J. Guckenheimer, M.R. Myers, F.J. Wicklin, P.A. Worfolk, Notices Amer. Math. Soc. 39 (1992) 303.
[19] T.B. Simpson, J.M. Liu, K.F. Huang, K. Tai, Quant. Semiclass. Opt. 9 (1997) 765.
[20] T.B. Simpson, private communications.